Mathematically modeling transient temperature variation in a human neonate undergoing intensive blue light phototherapy for management of hyperbilirubinemia

by
Vikram Baldini Gondhalekar

A THESIS

submitted to

Oregon State University

Honors College

in partial fulfillment of
the requirements for the
degree of

Honors Baccalaureate of Science in Bioengineering
(Honors Associate)

Presented May 26, 2017
Commencement June 2017

AN ABSTRACT OF THE THESIS OF

Vikram Baldini Gondhalekar for the degree of Honors Baccalaureate of Science in Bioengineering presented on May 26, 2017. Title: Mathematically modeling transient temperature variation in a human neonate undergoing intensive blue light phototherapy for management of hyperbilirubinemia.

Abstract approved:_____

Adam Higgins

Neonatal jaundice secondary to hyperbilirubinemia occurs in 60% of all term newborns and nearly all preterm newborns in the US. Severe cases of this may lead to chronic encephalopathy, neurologic deficits, and, in some cases, death. Intensive blue light phototherapy involves irradiation of a patient with high intensity light and is widely used for treatment of severe hyperbilirubinemia. Hyperthermia occurs in some neonates during intensive blue light phototherapy, and the cause of this is unclear. Body temperature of a hypothetical neonate undergoing intensive blue light phototherapy is mathematically modeled to investigate the cause of hyperthermia.

Key Words: neonate, hyperthermia, phototherapy, model, temperature

Corresponding e-mail address: gondhalv@oregonstate.edu

Mathematically modeling transient temperature variation in a human neonate undergoing intensive blue light phototherapy for management of hyperbilirubinemia

by
Vikram Baldini Gondhalekar

A THESIS

submitted to

Oregon State University

Honors College

in partial fulfillment of
the requirements for the
degree of

Honors Baccalaureate of Science in Bioengineering
(Honors Associate)

Presented May 26, 2017
Commencement June 2017

Honors Baccalaureate of Science in Bioengineering project of Vikram Baldini Gondhalekar presented on May 26, 2017.

APPROVED:

_____

Adam Higgins, Mentor, representing the Department of Chemical, Biological and Environmental Engineering

_____

Joseph McGuire, Committee Member, representing the Department of Chemical, Biological and Environmental Engineering

_____

Joe Baio, Committee Member, representing the Department of Chemical, Biological and Environmental Engineering

_____

Toni Doolen, Dean, Oregon State University Honors College

I understand that my project will become part of the permanent collection of Oregon State University, Honors College. My signature below authorizes release of my project to any reader upon request.

_____

Vikram Baldini Gondhalekar, Author

Mathematically modeling transient temperature variation in a human neonate undergoing intensive blue light phototherapy for management of hyperbilirubinemia

Student: Vikram B. Gondhalekar | *Mentor:* Adam Higgins Ph.D. | *Committee Members:* Joseph McGuire Ph.D. and Joe Baio Ph.D.

Introduction

I. Hyperbilirubinemia and associated pathophysiology

Unconjugated 4Z,15Z-bilirubin is a toxic and insoluble product of heme catabolism that does not readily exit the body. Bilirubin leaves the body after binding to glucuronic acid in the liver to form a water soluble compound (i.e. conjugated bilirubin), which can be excreted into the bile.

Blood vessels transport unconjugated bilirubin to the liver as bilirubin bound to albumin. Bilirubin dissociates from albumin in the liver, is rapidly internalized by hepatocytes, and binds to ligandin molecules inside the cells. Bilirubin and glucuronic acid conjugate in a reaction catalyzed by diphosphoglucuronyltransferase (UDPGT).

Indirect hyperbilirubinemia is defined as an abnormally elevated concentration of unconjugated bilirubin in the blood. Neonatal hyperbilirubinemia occurs in the majority of newborns. Two concurrent factors contribute to this prevalence. Firstly, fetal erythrocytes are rapidly broken down shortly postpartum, resulting in a rapid production of unconjugated bilirubin. Secondly, ligandin concentration and UDPGT activity are both below mature levels in the neonatal liver. Neonates with congenital liver disease, such as Gilbert Syndrome, are at an increased risk for severe hyperbilirubinemia.

Severe hyperbilirubinemia can cause chronic brain damage. Unconjugated bilirubin in the blood can transcend the blood brain barrier and accumulate in the central nervous system (CNS). Accumulation of bilirubin in the CNS can lead to permanent brain lesions, resulting in long-term neurologic disease and possibly death.

Details regarding bilirubin excretion, neonatal hyperbilirubinemia and bilirubin neurotoxicity are referenced from elsewhere [14] [12].

II. Blue light phototherapy

Blue light phototherapy is irradiation of a patient with light in the blue spectrum and is one of the most common treatments for neonatal hyperbilirubinemia. Blue light reacts with unconjugated 4Z,15Z-bilirubin bound to albumin to form lumirubin or 4Z,15E-bilirubin. Both products are water soluble and readily excreted into the bile without undergoing conjugation to glucuronic acid. Isomerization of unbound 4Z,15Z-bilirubin to 4E,15Z-bilirubin and oxidative degradation of 4Z,15Z-bilirubin also occur in the presence of blue light, however; these reactions are extremely rare in vivo. The formation of water soluble bilirubin isomers that are excreted from the body without reacting in the liver maintains the concentration of total bilirubin in the blood below levels that are concerning for neurotoxicity. Phototherapy is continued/repeated until the infant's liver function can meet

physiologic demand. Details of bilirubin photochemistry were referenced from Lamola [13].

III. Research Question

Intensive blue light phototherapy utilizes light in the 430-490 nm spectrum at a spectral irradiance ≥30 μW-cm^{-2}-nm^{1}, as defined by the American Pediatric Association (APA), and is applied in cases of severe hyperbilirubinemia [15] [4]. The highest level of spectral irradiance that can be safely used during intensive phototherapy is not established.

Hyperthermia occurs during intensive phototherapy and disrupts treatment. Phototherapy is discontinued if body temperature becomes ≥37.5 °C. This may necessitate the use of more invasive treatments, such as exchange transfusion, and may put the patient at a higher risk for bilirubin neurotoxicity.

A pediatric clinical investigation studied hyperthermia in neonates undergoing intensive blue light phototherapy. The study showed that there is a direct correlation between spectral irradiance and rise in body temperature of patients undergoing phototherapy. Moreover, the body temperature of every patient included in the study who was irradiated with blue light at a spectral irradiance ≥60 μW-cm^{-2}-nm^{-1} became ≥37.5 °C [4].

The advent of hyperthermia during intensive phototherapy creates challenges in the clinical setting. Irradiating the patient with high intensity light may lead to hyperthermia, however; less intense phototherapy may be inadequate in severe cases of hyperbilirubinemia. The ambiguity surrounding the upper limit of spectral irradiance that is safe to use exacerbates the problem. These challenges may lead to less than optimal care for patients at risk of debilitating chronic sequelae, motivating an investigation into the source of hyperthermia during phototherapy and strategies to avoid it.

The cause/s of hyperthermia during phototherapy are not well understood. Absorption of light heats the patient. However, there is evidence that a pyrogenic cytokine mediated inflammatory response occurs during intensive blue light phototherapy, and this may cause body temperature to rise as well [4]. It remains unclear which of these events, if either, is the prevailing cause of hyperthermia during intensive phototherapy.

IV. Project Objective

The goal of this project is to help identify the principal cause of hyperthermia in neonates undergoing intensive blue light phototherapy. The body temperature of a hypothetical neonate is mathematically modeled to possibly accomplish this.

The model assess the rise in patient body temperature that occurs due to absorption of blue light. The model does not consider heat producing biologic processes possibly triggered during phototherapy. This study may help rule out or confirm blue light absorption as the primary cause of hyperthermia during phototherapy.

Separately, it is felt that the present study may contribute to thermal modeling of neonates in the future. Much research has been devoted to modeling temperature variation in adults [18]. However, few if any attempts were made at modeling full body temperature variation in neonates. This study seeks to consolidate the neonate system with work done by others to model temperature within the human body. This may facilitate thermal modeling of neonates in other biomedical settings.

Mathematical Model

I. Physical system and surroundings

The development of the model begins by simplifying the neonate geometry, assigning physical quantities to each tissue group, assuming an initial temperature profile and describing the neonate's surroundings. Figure 1 is an illustration of the system and surroundings.

The geometry of a supine neonate body is simplified to a single circular cylinder. Other thermal models of the human body use similar geometries [8] [11]. The total mass of the cylinder is set equal to 3.2 kg, the average mass of a neonate [16]. The average height of a neonate is 0.50 m [16]. The body surface area (*BSA*) of the average neonate is approximated by inputting the previously stated values of height and mass into the Meban formula [1]. The value of this is 0.21 m^2 and is set equal to the lateral surface area of the cylinder. Dividing the total mass of the cylinder by the average density of a neonate gives the total volume of the cylinder, equal to 3100 cm^3 [10]. The volume and lateral surface area of the cylinder are used to calculate its length and the cross sectional radius. These are 1.1 m and 3 cm, respectively.

The cylinder is divided into six parts, a central cylinder circumscribed by five shells. Each part represents a different tissue type within the simplified neonate body. It is assumed that there is perfect thermal contact between each tissue group and the tissue groups adjacent to it.

The body parts considered here and in other thermal models of the human body are the cortex, brain stem, cervical medulla, thoracic medulla, liver, kidney, stomach, gut, bladder, thyroid gland, spleen, esophagus, trachea, lungs, heart, blood, bone, muscle, connective tissue, fat and skin [8] [24].

The mass fractions of bone, muscle, connective, fat and skin tissue are higher than for other body parts, and these tissues are closest to the surface of the body per data obtained by others [8] [24]. Each of these is represented by one of the shells separating the central cylinder from the surroundings. The bone shell is in direct contact with the central cylinder and is surrounded by muscle, connective, fat, and skin tissue, mentioned in the order of increasing distance from the central cylinder. A thermal model done by Ferreira and Yanagihara uses a similar configuration [8]. The values of physical/properties (e.g. thermal conductivity, density, etc…) and basal metabolic heat production characteristic of each tissue are referenced from empirical studies that measured these values using adult tissue and used here [24]. The volume of each shell is calculated by multiplying the volume fraction of the tissue that shell represents by the total volume of the simplified neonatal body. The volume fraction of each tissue is referenced from empirical studies that measured this in the adult body [24].

The remaining body parts are labeled core structures. These are represented by the central cylinder, which is composed of a hypothetical tissue type labeled "core tissue". Gage, Stolwijk, and Nishi used a similar treatment [11]. The change in core tissue temperature approximates the average change in temperature of core structures within the body. The volume of the central cylinder is equal to the sum of the volume fractions of each body part represented by the central cylinder multiplied by the total volume of the simplified neonatal body. Volume fractions of each body part used here were measured in

the adult system by others [24]. The mass weighted mean of each physical property pertinent to the model is averaged over all body parts that make up the core and set equal to the value of that physical property in the core tissue. Values of physical properties used in this calculation were measured using adult tissue. This is similar to what was done for the more peripheral tissue groups [24].

Values of physical quantities characteristic of neonatal tissue and volume fractions of body parts in neonates are not available in the literature to the authors' best knowledge.

The radius of the central cylinder and the outer radius of each shell is calculated using the volume of each shell and the length of the body. Dimensions of the central cylinder and shells as well as the physical properties of each tissue are listed in Table 1 and Table 2. The density and specific heat capacity of blood are also listed in Table 1 and are used when evaluating convective heat exchange between the tissue and blood in the microvasculature.

All tissue groups are assumed to be at an initial temperature of 37 °C.

The simplified neonate body lays in a hypothetical incubator on top of a blanket. The blanket covers half the *BSA*. The incubator walls surround the body. The air inside the incubator is saturated with water. The temperature of the blanket, walls, and air is set to a constant 33 °C, equal to the average temperature of a neonate incubator during blue light phototherapy measured in the clinical setting [4]. Matter outside the incubator is not considered. A source of blue light exists above the cylinder and irradiates the top half of the cylinder with light in the 430-490 nm spectrum (the region of blue light used in the definition of intensive blue light phototherapy put forth by the APA) at a constant spectral irradiance. No other sources of visible light are present. The blue light source is far from the infant, and non-radiative heat generated by the light source is not considered. The specifications used here reflect the incubator environment as described by clinical researchers [4].

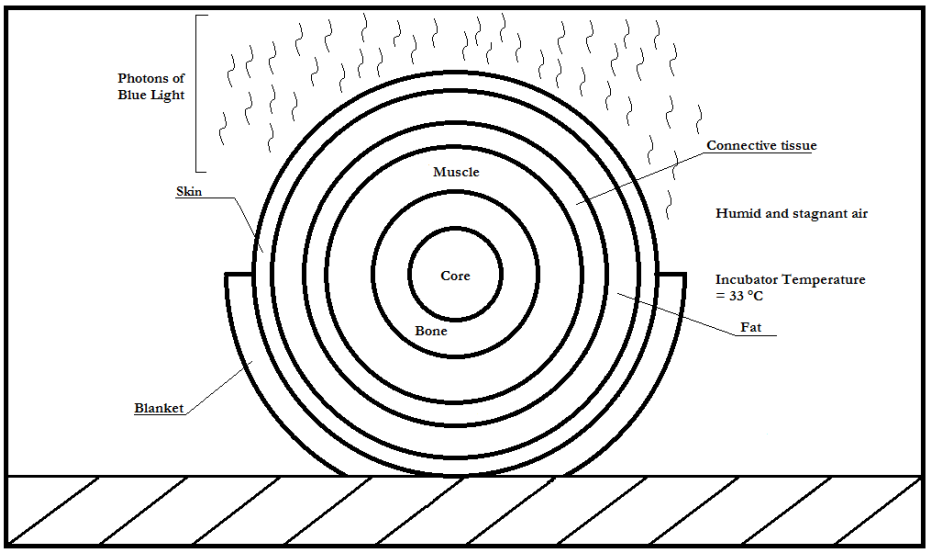

Figure 1. The neonate body approximated as a cylinder made up of a central cylinder and five concentric shells. The cross section of the cylinder in a hypothetical incubator is shown here. The illustration is not to scale. The central cylinder is made up of core tissue. The shells represent bone, muscle, connective, fat and skin tissue. Blue light irradiates the upper half of the body at constant spectral irradiance. Surrounding air is at a temperature of 33 °C and stagnant. Humidity of air is 1. The rectangular perimeter represents the plastic walls of the incubator. The walls of the incubator surround the body. The insulating material under and around the cylinder is the blanket. Matter outside the incubator is not considered. No other sources of light are considered.

Table 1. Dimensions of the central cylinder that represent core tissue and the shells that represent bone, muscle, connective, fat, and skin tissue. Density and specific heat capacity of each tissue are shown. The values of these in blood are also shown. Values of density and heat capacity were referenced from others who measured these in adults [24].

Tissue Type	Volume [cm^3]	Outer Radius [cm]	Density [kg/m^3]	Specific Heat Capacity [J/kg-K]
Core	471	1.2	970	3650
Bone	372	1.6	1520	1700
Muscle	1400	2.5	1085	3800
Connective	214	2.6	1085	3200
Fat	502	2.9	920	2300
Skin	164	3	1085	3680
Blood	-	-	1059	3850

Table 2. Thermal conductivity, basal blood perfusion rate and basal metabolic heat production in core, bone, muscle, connective, fat and skin tissue. Values were referenced from others who measured these in the adult body [24].

Tissue Type	Thermal Conductivity [W/m-K]	Basal Blood Perfusion Rate [m^3_{blood}/m^3_{tissue} x 10^6]	Basal Metabolic Heat Production [W/m^3]
Core	0.47	1800	828
Bone	0.65	0	368
Muscle	0.51	543	684
Connective	0.47	100	369
Fat	0.21	77	300
Skin	0.47	362	368

II. General Model Development

The goal of this section is to develop a differential equation describing temperature variation within the simplified neonate body as a function of time and position. The development focuses on an arbitrary point and is generalizable to any point within the body.

An arbitrary point in the body is treated as a closed thermodynamic system. The temperature of the system relates to its internal energy. Change in internal energy over time is equal to the net rate of heat entering the system and the net rate of work done on the system. This equivalence is an energy balance derived from the first law of thermodynamics. Its mathematical form is:

$$\frac{dU}{dt} = H + W \quad (Eq. 1.1)$$

where dU is change in internal energy, dt is change in time, H is net rate of heat entering the system and W is net rate of work done on the system.

The following assumptions are applied: work is not done, bulk kinetic energy is constant, and potential energy is constant. Considering these, the specific heat formula relates change in temperature to change in internal energy. Applying the stated assumptions and incorporating the specific heat formula into the energy balance gives:

$$\frac{d(m * C_P * T)}{dt} = H \quad (Eq. 1.2)$$

where m is mass, C_p is specific heat, and T is temperature.

The temperature at a single point in the body is assumed to be independent of longitudinal position and azimuth angle. Assuming this, the energy balance taken around a single point is equivalent to an energy balance taken around an infinitesimally thin shell that encompasses that point and that extends down the central axis of the cylindrical body. Figure 2 illustrates the transverse cross section of such a shell. The remainder of the development considers the energy balance taken around the thin shell.

Applying equation 1.2 to the shell, the value of H is equal to the net rate of heat entering and leaving the shell and the net rate of heat generated and consumed within the shell. Qualitatively incorporating this into the energy balance gives:

$$\frac{d(m * C_P * T)}{dt} = Heat_{(In-Out)} + Heat_{(Generation-Consumption)} \quad (Eq. 1.3)$$

Net basal metabolic heat production (B) multiplied by the volume (V) of the shell gives the net heat generated and consumed within the shell. B is assumed constant, recalling that biologic processes possibly triggered during phototherapy are not considered here.

$$Heat_{(Generation-Consumption)} = B * V \quad (Eq. 1.4)$$

Heat enters and leaves the shell via convective, radiative and conductive heat transfer. It is assumed that heat transfer does not occur at the circular ends of the cylindrical body.

$$Heat_{(In-Out)} = Convective\ HT + Radiative\ HT + Conductive\ HT \quad (Eq. 1.5)$$

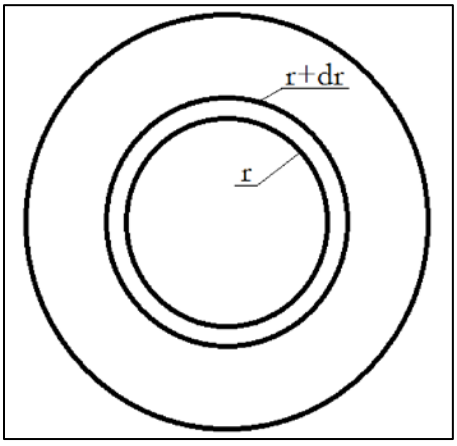

Figure 2. The cross section of an arbitrary infinitesimally thin shell within the simplified neonatal body. An energy balance taken around such a shell is equivalent to the energy balance taken around any point encompassed by the shell, assuming that temperature does not vary with polar position or azimuthal angle.

Convective heat transfer is written as a function, Q, multiplied by the volume of the shell.

$$Convective\ HT = Q * V \quad (Eq. 1.6)$$

Convective heat transfer is typically treated as a function of the surface area of the system. The model of convective heat transfer within the body used by others and applied in this study necessitates the contrasting treatment used here and is discussed later.

Radiative heat transfer is described as function *R* multiplied by the surface area (*A*) of the shell. Net radiative heat exchange is the difference of this product evaluated at the inner and outer layer of the shell. The is expresses as:

$$Radiative\ HT = (R * A)_{r+dr} - (R * A)_r \quad (Eq. 1.7)$$

Fourier's Law describes conductive heat transfer and is:

$$J = -k * \nabla T \quad (Eq. 1.8)$$

where *J* is conductive heat flux, *k* is thermal conductivity, and ∇T is the three dimensional temperature gradient. ∇T simplifies to a derivative of temperature with respect to radial position, recalling the assumption that temperature does not vary with longitudinal position or azimuth angle.

$$J = -k * \frac{dT}{dr} \quad (Eq. 1.9)$$

The difference in Fourier's Law multiplied by the surface area of the shell evaluated at the outer and inner surface of the shell gives the rate of heat entering and leaving the shell via conductive heat transfer.

$$Conductive\ HT = \left(-k * \frac{dT}{dr} * A\right)_{r+dr} - \left(-k * \frac{dT}{dr} * A\right)_r \quad (Eq. 1.10)$$

Substituting the generation and consumption term and heat transfer terms into the energy balance equation and re-writing the equation in partial differential notation gives:

$$\frac{\partial(m * C_P * T)}{\partial t} = \left(-k * \frac{\partial T}{\partial r} * A\right)_{r+dr} - \left(-k * \frac{\partial T}{\partial r} * A\right)_r + (R * A)_{r+dr} - (R * A)_r + Q * V + B * V \quad (Eq. 1.11)$$

Density, heat capacity, and volume are assumed to be independent of time. Re-writing the mass of the shell as the product of volume and density and dividing by the common volume term gives:

$$\rho * C_P \frac{\partial(T)}{\partial t} = \frac{\left(-k * \frac{\partial T}{\partial r} * A\right)_{r+dr} - \left(-k * \frac{\partial T}{\partial r} * A\right)_r}{V} + \frac{(R * A)_{r+dr} - (R * A)_r}{V} + Q + B \quad (Eq. 1.12)$$

Re-writing *A* and *V* in terms of *r* and the length of the cylindrical body (*L*) and factoring out constant common monomials from the radiative and conductive heat transfer terms gives:

$$\rho * C_P \frac{\partial(T)}{\partial t} = \frac{2 * \Pi * L * (\left(-k * r \frac{\partial T}{\partial r}\right)_{r+dr} - \left(-k * r \frac{\partial T}{\partial r}\right)_r + (R * r)_{r+dr} - (R * r)_r)}{\Pi * (r + dr)^2 * L - \Pi * r^2 * L} + Q + B \quad (Eq. 1.13)$$

Cancelling out common factors gives:

$$\rho * C_P \frac{\partial(T)}{\partial t} = \frac{2}{(2r + dr)} \frac{(\left(-k * r \frac{\partial T}{\partial r}\right)_{r+dr} - \left(-k * r \frac{\partial T}{\partial r}\right)_r)}{dr} + \frac{2}{(2r + dr)} \frac{((R * r)_{r+dr} - (R * r)_r)}{dr} + Q + B \quad (Eq. 1.14)$$

The difference in conductive and radiative heat transfer at the inner and outer surface of the shell is re-written in differential form, recognizing that *dr* is infinitesimally small.

$$\rho * C_P \frac{\partial(T)}{\partial t} = \frac{1}{r} * \frac{\partial}{\partial \mathrm{r}}\left(-k * r \frac{\partial T}{\partial r}\right) + \frac{1}{r} * \frac{\partial}{\partial \mathrm{r}}(R * r) + Q + B \quad (Eq. 1.15)$$

Equation 1.15 is an energy balance that is generalizable to the entire simplified body. However, the abrupt changes in tissue type that occur along the radial direction causes discontinues in the energy balance taken around the entire body. This is addressed by applying a separate energy balance equation to the core, bone, muscle, connective, fat, and skin tissue separately.

Integrating the final form of the energy balance within each tissue group gives the spatial and temporal temperature profile within the simplified neonatal body. Others derived similar equations [21]. The following subsections expand on the terms *Q* and *R*. Terms describing convective and radiative heat exchange with the surroundings and evaporative heat loss from the skin are also described in the following sections. Heat exchange between the skin and surroundings are incorporated into the energy balance when the energy balance is evaluated at the surface of the skin.

III. Convective Heat Transfer

The sum of the terms described in this subsection make up the function *Q*. Note that heat exchange coefficients between the skin and the environment are only included in *Q* when the energy balance is evaluated at the surface of the skin.

Heat exchange between tissue and blood: Pennes proposed a function describing convective heat transfer between a unit volume of tissue and blood in the microvasculature [18]. This equation is widely used in the literature [8] [11] [21]. Its general form is:

$$B_{micro} = \omega_{bl} * \rho_{bl} * c_{bl} * (T_{ar} - T_v) \quad (Eq. 1.16)$$

where $B_{micro,}$ is heat exchange between the tissue and blood in the capillaries per unit volume of tissue, ω_{bl} is basal blood perfusion rate through the tissue per unit volume of tissue, ρ_{bl} is the density of blood, c_{bl} is the heat capacity of blood, T_{ar} is the temperature of arterial blood entering the tissue, and T_v is the temperature of venous blood flowing out of the tissue element. Note that this approach treats convective heat exchange as a function of volume rather than surface area.

The temperature of blood is assumed to equilibrate with the temperature of the tissue before the blood exists the tissue element. This assumption was proposed by Pennes and supported in an analysis done by Chen [6]. Applying this assumption to the heat exchange equation gives:

$$B_{micro} = \omega_{bl} * \rho_{bl} * c_{bl} * (T_{ar} - T) \quad (Eq. 1.17)$$

Temperature of arterial blood entering the core tissue is set equal to the weighted average of the temperature of blood exiting the other tissue groups. The temperature of arterial blood entering tissue groups other than the core is set equal to the average temperature of the core tissue. This treatment is similar to that done by Gage, Stolwijk, and Nishi [11]. Heat transfer due to bulk blood flow is not considered. Basal blood perfusion is assumed to be constant for a given tissue type.

Convective heat transfer with the surroundings: Convective heat exchange occurs between the skin and the surrounding air over half of the *BSA* (the surface area of the skin not covered by the blanket). An expression describing rate of heat transfer between the skin and bulk air was developed by others and shown here [11].

$$C_{surr} = h * (T_s - T_\infty) * 0.50 * BSA \quad (Eq. 1.18)$$

where C_{surr} is the heat flux secondary to convective heat transfer with the surrounding air, h is the overall heat transfer coefficient, T_s is the value of temperature at the skin surface, and T_∞ is the temperature of the bulk air.

There is no forced flow of air and bulk air temperature is assumed constant at 33 °C. Others measured the overall heat transfer coefficient pertaining to convective heat exchange between a nude neonate mannequin and stagnant air in an incubator environment to be 4.94 W/m^2-K [3]. This value is assumed to be constant.

IV. Radiative heat transfer

The sum of the terms described in this subsection make up the function *R*. In each circumstance, it is assumed that all the radiative energy absorbed by the skin takes on the form of heat. *R* includes terms describing blue light absorption and radiative heat exchange with the environment when the energy balance is evaluated at the surface of the skin.

Blue light absorption: The following integral quantifies blue light absorbed by the skin:

$$R_b = \int_{\lambda_i}^{\lambda_f} (I * \alpha(\lambda, \theta, \varphi)) d\lambda \quad (Eq. 1.19)$$

where R_b is energy flux, I is spectral irradiance and α is monochromatic absorptivity of skin written as a function of the wavelength of incident light (λ), polar angle of incidence (θ), and azimuthal angle of incidence (φ). The blue light source emits radiation in the spectrum bounded by λ_i and λ_f.

The following equation relates absorptivity to reflectance (γ) and transmittance (τ):

$$1 = \alpha(\lambda, \theta, \varphi) + \tau(\lambda, \theta, \varphi) + \gamma(\lambda, \theta, \varphi) \quad (Eq. 1.20)$$

Assuming that transmittance of blue light through the skin is negligible allows the absorption integral to be re-written as:

$$R_b = \int_{\lambda_i}^{\lambda_f} I * (1 - \gamma(\lambda, \theta, \varphi)) d\lambda \quad (Eq. 1.21)$$

It is assumed that the skin reflects blue light diffusely. This is expressed as:

$$\gamma(\lambda, \theta, \varphi) \approx \overline{\gamma(\lambda)} \; for \; all \; \theta \; and \; \varphi \quad (Eq. 1.22)$$

Anderson and Parrish used an integrating sphere to measure diffuse reflectivity as a function of wavelength in the blue spectrum [2]. Nielsen et al. modeled diffuse reflectivity of skin in the blue spectrum for different concentrations of cutaneous melanin. Their model is consistent with the measurements done by Anderson and Parrish [17]. Reflectivity of skin (7.5% melanin) is written as a function of wavelength in the spectrum of 430-490 nm using predications made by Nielsen et al. This correlation is:

$$\overline{\gamma(\lambda)} = 9 * 10^{-6} * \lambda^2 - 0.0074 * \lambda + 1.6589 \quad (Eq. 1.23)$$

where wavelength is expressed in units of nm. This function is substituted into the absorption integral, and a definite integral is taken from 430 to 490 nm:

$$R_b = \int_{430\,nm}^{490\,nm} I * \left(1 - (9 * 10^{-6} * \lambda^2 - 0.0074 * \lambda + 1.6589)\right) d\lambda \quad (Eq. 1.24)$$

Evaluating the integral while treating spectral irradiance as a constant gives:

$$R_b = I * 50.28 \quad (Eq. 1.25)$$

Recalling that blue light is incident on the top half of the neonate, the total heat entering the skin via absorption of blue light radiation (R_B) is:

$$R_B = \frac{BSA}{2} * I * 50.28 \quad (Eq. 1.26)$$

Radiation emitted by the surroundings: Radiation emitted by the plastic walls of the incubator and the blanket is absorbed by and heats the skin. The following integral quantifies the radiation emitted by the wall and the blanket and absorbed by the skin per unit surface area of skin:

$$R_{surr} = \int_0^{\infty} (M_{surr} * \alpha(\lambda, \theta, \varphi)) d\lambda \quad (Eq. 1.27)$$

where R_{surr} is energy flux and M_{surr} is monochromatic emissive power of the walls and blanket. Skin absorptivity is assumed constant over the domain of wavelength while evaluating this integral. This is discussed later in this subsection. Applying this assumption to the absorption integral gives:

$$R_{surr} = \alpha * \int_0^{\infty} M_{surr}\, d\lambda \quad (Eq. 1.28)$$

It is assumed that the black body model reasonably approximates the radiation emitted by the plastic walls and blanket. Given this, the integral of monochromatic emissivity over the domain of wavelength is equal to the Stefan-Boltzmann law.

$$R_{surr} = \alpha * \sigma * T_{\infty}^4 \quad (Eq. 1.29)$$

where T_∞ is the temperature of the walls and blanket and σ is the Stefan Boltzmann constant. T_∞ is set to 33 °C and constant, as mentioned before.

Integrating Planck's Law over the infrared (IR) region shows that 99% of the radiation emitted by a black body at 33 °C is within the IR band. To the author's best knowledge, measurements of skin absorptivity are limited to a narrow band of wavelengths, and there is no outstanding model of skin absorptivity in the IR region. Given this, absorptivity is assumed to be one and constant. This assumption should be revisited when more empirical data is available. Applying this assumption gives:

$$R_{surr} = \sigma * T_{\infty}^4 \quad (Eq. 1.30)$$

The incubator walls and the blanket circumscribe the neonate body, and a view factor of one is assumed. The total heat entering the neonate as radiation emitted by the walls and blanket ($R_{surr,total}$) is:

$$R_{surr,total} = BSA * \sigma * T_{\infty}^4 \quad (Eq. 1.31)$$

Radiation emitted within the body and at the surface of the skin: Radiative heat transfer occurs within the body and at the surface of the skin. Assuming that radiation emitted by all tissue types is diffuse, the following integral gives the radiative heat emitted at each point within the body per unit area:

$$R_t = \int_0^{\infty} (\epsilon_\lambda * P(\lambda, T)) d\lambda \quad (Eq. 1.32)$$

where R_t is flux, ϵ_λ is monochromatic emissivity and $P(\lambda,T)$ is Planck's Law as a function of wavelength and temperature within the body.

Sanchez et al. measured the monochromatic emissivity of skin to be nearly one in the IR region from 3000 to 14000 nm and near constant [20]. Others obtained similar values [22]. Given these findings, it is assumed that one approximates the emissivity of skin throughout the IR band. Furthermore, over 99% of radiation emitted by a black body at a temperature of 33-39 °C exists within the IR band. Given this, it is assumed that the Stefan-Boltzmann Law reasonably approximates the total radiative power emitted by the neonatal skin.

Unfortunately, similar measurements of emissivity in other tissue types are not available in the literature. Given this, the model assumes that all tissue types emit like a black body.

Applying these assumptions and evaluating the integral over the domain of wavelength gives the Stefan-Boltzmann Law:

$$R_t = \sigma * T^4 \quad (Eq. 1.33)$$

V. Heat exchange due to evaporation of water

Evaporative heat loss from the surface of the skin (E_{sk}) is the sum of heat lost due to water diffusing through the skin (E_{diff}) and vaporization of secreted sweat (E_{sw}). This is mathematically expressed as:

$$E_{sk} = E_{diff} + E_{sw} \quad (Eq. 1.34)$$

Attempts to model sweat production as a function of temperature in the neonate body are not widespread in the literature, and this model does not consider evaporation of sweat. The value of E_{diff} is calculated using the following formula referenced from Gage, Stolwijk, and Nishi [11]:

$$E_{sk} = E_{diff} = w_{diff} * \kappa * h * (P_{sk} - \phi_a * P_a) * F_{pcl} \quad (Eq. 1.35)$$

where w_{diff} is a dampness factor equal to 0.06, κ is a proportionality constant equal to 2.2 °C/mmHg, h is the overall heat transfer coefficient previously used to describe convective heat exchange between the skin and bulk air, P_{sk} is vapor pressure of water at skin temperature in mmHg, ϕ_a is the relative humidity, P_a is vapor pressure at bulk air temperature in mmHg, and F_{pcl} is the permeation efficiency of water through clothes, equal to 1 in the current assessment of a nude neonate.

The air in the incubator is saturated with water (relative humidity is one). P_a is equal to 37.7 mmHg and constant, recalling the assumption that bulk air temperature is constant at 33 °C. The Antoine equation approximates the value of P_{sk} in units of mmHg as a function of mean skin temperature ($T_{skin,avg}$) in units of °C. This is:

$$P_{sk} = 10^{8.07 - \frac{1730.63}{233.43 + T_{skin,avg}}} \quad (Eq. 1.36)$$

Substituting the Antoine equation into the formula for evaporative heat loss through the skin and multiplying this by the *BSA* of the neonate gives the rate of heat loss due to diffusion of water through the skin.

$$E_{sk} = BSA * w_{diff} * \kappa * h * \left(10^{8.07 - \frac{1730.63}{233.43 + T_{skin,avg}}} - \phi_a * P_a\right) \quad (Eq. 1.37)$$

Model Solution

The energy balance presented in the previous section is numerically integrated using the finite volume method. This technique is applied in other temperature models of the human body and to other heat and fluid transport problems [21] [5]. The general treatment is developed here and applied separately to each tissue group inside the neonate body.

The general form of the finite volume method applied to a cylindrical body begins by discretizing the cylinder into n number of equally spaced finite concentric shells. The shells are numbered from 1 to n in the order they extend away from the center of the cylinder. The symbol i is an integer between 1 and n and denotes an arbitrary shell in the series. The symbol r_i denotes the radius of the circle that bounds the outer perimeter of i^{th} shell. The

symbol p_i denotes a point that lies midway between the inner and outer bounds of the i^{th} shell in the radial direction. The width of each shell is equal to Δr. Figure 3 illustrates this discretization, using a half the cylinder for better visualization.

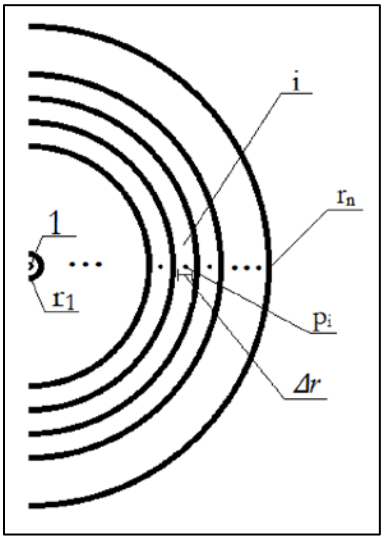

Figure 3. A half cylinder discretized into *n* number of uniform thin concentric shells. The shells are numbered from 1 to *n* in the order they extend outwards in the radial direction. The variable Δr is the width of each shell. The i^{th} shell is an arbitrary shell in the series. The variable r_i represents the outer radius of the i^{th} shell, and the variable p_i represents the midpoint of the i^{th} shell in the radial direction.

The solution of the energy balance taken around the i^{th} shell is developed and is generalizable to all finite elements in the discretized body. Figure 4 gives a local view of the i^{th} shell. The final form of the energy balance presented in the Model Development section is:

$$\rho * C_P \frac{\partial T}{\partial t} = \frac{1}{r} * \frac{\partial}{\partial \mathrm{r}}\left(-k * r \frac{\partial T}{\partial r}\right) + \frac{1}{r} * \frac{\partial}{\partial \mathrm{r}}(R * r) + Q + B \quad (Eq.\,1.15)$$

A definite double integral is taken over the time interval $[t_i, t_f]$ and the volume of the i^{th} shell.

$$\int_{V_{i-1}}^{V_i}\int_{t_i}^{t_f}\left(C_P * \rho * \frac{\partial T}{\partial t}\right) dtdV$$

$$= \int_{V_{i-1}}^{V_i}\int_{t_i}^{t_f}\left(\frac{1}{r} * \frac{\partial\left(-k * r \frac{dT}{dr}\right)}{\partial r}\right) dtdV + \int_{V_{i-1}}^{V_i}\int_{t_i}^{t_f}\frac{1}{r} * \frac{\partial}{\partial \mathrm{r}}(R * r)\, dtdV + \int_{V_{i-1}}^{V_i}\int_{t_i}^{t_f} Q\, dtdV$$

$$+ \int_{V_{i-1}}^{V_i}\int_{t_i}^{t_f} B\, dtrdr \quad (Eq.\,2.1)$$

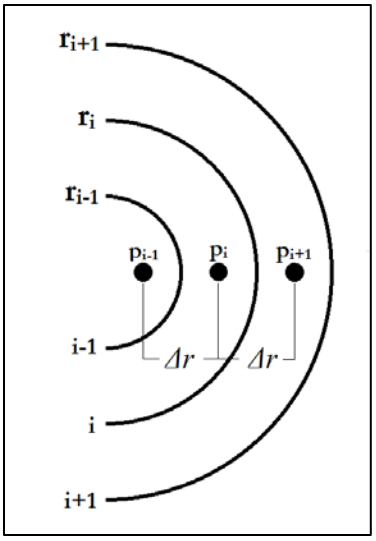

Figure 4. The i^{th} shell and its corresponding radius and midpoint. Shells adjacent to the i^{th} shell are shown. The midpoint of each shell is a distance Δr from the midpoint of the adjacent shell in both directions. An energy balance is developed around the i^{th} shell.

The volume of the thin shell is approximated as:

$$dV = dr * rd\theta * dz \quad (Eq. 2.2)$$

This is substituted into the energy balance, the polar and azimuthal terms are cancelled out, recalling that temperature is independent of these dimensions, and the common r factor in the radiative and conductive terms are cancelled out.

$$\int_{r_{i-1}}^{r_i}\int_{t_i}^{t_f}\left(C_P * \rho * \frac{\partial T}{\partial t}\right) dtrdr = \int_{r_{i-1}}^{r_i}\int_{t_i}^{t_f}\left(\frac{\partial\left(-k * r\frac{dT}{dr}\right)}{\partial r}\right) dtdr + \int_{r_{i-1}}^{r_i}\int_{t_i}^{t_f}\partial(R * r)\, dt + \int_{r_{i-1}}^{r_i}\int_{t_i}^{t_f} Q\, dtrdr + \int_{r_{i-1}}^{r_i}\int_{t_i}^{t_f} B\, dtrdr \quad (Eq. 2.3)$$

It is assumed that temperature does not vary with respect to radial position within the finite shell. Applying this assumption, the spatial integral is evaluated for all terms aside from the conduction and radiation terms.

$$\frac{({r_i}^2 - {r_{i-1}}^2)}{2} * \int_{t_i}^{t_f}\left(C_P * \rho * \frac{\partial T}{\partial t}\right) dt = \int_{r_i-1}^{r_i}\int_{t_i}^{t_f}\left(\frac{\partial\left(-k * r\frac{dT}{dr}\right)}{\partial r}\right) dtdr + \int_{r_{i-1}}^{r_i}\int_{t_i}^{t_f}\partial(R * r)\, dt + \frac{({r_i}^2 - {r_{i-1}}^2)}{2} * \int_{t_i}^{t_f} Q\, dt + \frac{({r_i}^2 - {r_{i-1}}^2)}{2} * \int_{t_i}^{t_f} B\, dt \quad (Eq. 2.4)$$

Re-arranging:

$$\int_{t_i}^{t_f}\left(C_P * \rho * \frac{\partial T}{\partial t}\right)dt = \frac{2}{({r_i}^2 - {r_{i-1}}^2)} * \int_{r_{i-1}}^{r_i}\int_{t_i}^{t_f}\left(\frac{\partial\left(-k * r\frac{dT}{dr}\right)}{\partial r}\right)dtdr + \frac{2}{({r_i}^2 - {r_{i-1}}^2)} * \int_{r_{i-1}}^{r_i}\int_{t_i}^{t_f}\partial(R * r)\,dt + + \int_{t_i}^{t_f} Q\,dt + \int_{t_i}^{t_f} B\,dt \quad (Eq.2.5)$$

The net rate of radiative heat entering the i^{th} shell is the radiative power emitted by the i-1 shell across r_{i-1} and i+1 shell across r_i subtracted by the radiative power emitted by the i^{th} shell across both r_{i-1} and r_i. Applying this gives:

$$\int_{t_i}^{t_f}\left(C_P * \rho * \frac{\partial T}{\partial t}\right)dt = \frac{2}{({r_i}^2 - {r_{i-1}}^2)} * \int_{r_{i-1}}^{r_i}\int_{t_i}^{t_f}\left(\frac{\partial\left(-k * r\frac{dT}{dr}\right)}{\partial r}\right)dtdr + \frac{2}{({r_i}^2 - {r_{i-1}}^2)} * \int_{t_i}^{t_f}\left(r_i * (R_{i+1} - R_i) - r_{i-1} * (R_i - R_{i-1})\right) + \int_{t_i}^{t_f} Q\,dt + \int_{t_i}^{t_f} B\,dt \quad (Eq.2.6)$$

The time integral of the partial derivative of temperature with respect to time is the difference in temperature at time t_f and the temperature at time t_i. Recalling that heat capacity and density are assumed constant, this gives:

$$C_P * \rho * \left(T|_{t_f} - T|_{t_i}\right) = \frac{2}{({r_i}^2 - {r_{i-1}}^2)} * \int_{r_{i-1}}^{r_i}\int_{t_i}^{t_f}\left(\frac{\partial\left(-k * r\frac{dT}{dr}\right)}{\partial r}\right)dtdr + \frac{2}{({r_i}^2 - {r_{i-1}}^2)} * \int_{t_i}^{t_f}\left(r_i * (R_{i+1} - R_i) - r_{i-1} * (R_i - R_{i-1})\right) + \int_{t_i}^{t_f} Q\,dt + \int_{t_i}^{t_f} B\,dt \quad (Eq.2.7)$$

The derivative of temperature with respect to radius at r_i is approximated as the difference between temperature at the point p_{i+1} and the point p_i divided by Δr. Similarly, the derivative of temperature with respect to radius at r_{i-1} is approximated as the difference between temperature at point p_i and the point p_{i-1} divided by Δr. Applying this assumption and treating k as a constant, the spatial integral of Fourier's Law is evaluated:

$$C_P * \rho * \left(T|_{t_f} - T|_{t_i}\right) = \frac{-2 * k}{({r_i}^2 - {r_{i-1}}^2)} * \int_{t_i}^{t_f}\left(r_i * \frac{T|_{p_{i+1}} - T|_{p_i}}{\Delta r} - r_{i-1} * \frac{T|_{p_i} - T|_{p_{i-1}}}{\Delta r}\right)dt + \frac{2}{({r_i}^2 - {r_{i-1}}^2)} * \int_{t_i}^{t_f}\left(r_i * (R_{i+1} - R_i) - r_{i-1} * (R_i - R_{i-1})\right) + \int_{t_i}^{t_f} Q\,dt + \int_{t_i}^{t_f} B\,dt \quad (Eq.2.8)$$

The time integrals on the right hand side of the equation are evaluated by taking explicit Riemann sum approximations. Applying this and re-writing the difference between t_f and t_i as Δt gives:

$$C_P * \rho * \left(T|_{t_f} - T|_{t_i}\right) = \frac{-2 * k * \left(\left(r_i * \frac{T|_{p_{i+1}} - T|_{p_i}}{\Delta r} - r_{i-1} * \frac{T|_{p_i} - T|_{p_{i-1}}}{\Delta r}\right) dt\right) * \Delta t}{(r_i{}^2 - r_{i-1}{}^2)} + \frac{2 * \Delta t * \left(r_i * (R_{i+1} - R_i) - r_{i-1} * (R_i - R_{i-1})\right)}{(r_i{}^2 - r_{i-1}{}^2)} + \Delta t * Q + \Delta t * B \quad (Eq. 2.9)$$

This formula approximates the temporal temperature profile of the i^{th} shell. The accuracy of the approximation improves as n becomes larger and Δt becomes smaller. The solution is applied to each volume element in the discretized system.

The finite volume method is applied separately to the core, bone, muscle, connective, fat, and skin tissue to obtain the spatial-transient temperature profile in each tissue group.

Special consideration must be taken when applying the approximate integral of the energy balance to the 1st and n^{th} element in each tissue group. For all tissue types aside from the skin, the n^{th} shell is below and adjacent to a shell representing a different tissue type. Consequently, heat exchange across the upper bound of each n^{th} shell is dependent on the temperature of the n^{th} shell as well as the temperature of the 1st shell in the tissue group that lies above it. This is conversely true for the 1st element in each tissue group aside from the core tissue.

The n^{th} shell of the skin tissue lies at the interface of the body and the incubator environment. R and Q include terms describing radiative and convective heat exchange with the environment when the solution of the energy balance is applied to the n^{th} shell of the skin. Conductive heat exchange between the skin and the blanket is dependent on the temperature of the n^{th} shell of the skin and the constant temperature of the blanket. Conductive heat exchange between the blanket and the skin occurs over half of the outer lateral surface area of the skin.

Considerations/Limitations

The model may exaggerate the effect of blue light absorption on core temperature. Assumptions made during the development of the model minimize heat sinks in the surroundings. The incubator walls and the blanket emit radiation like black bodies. It is assumed that the absorptivity of neonatal skin in the IR spectra is one. Air is assumed stagnant and saturated with water. Evaporation of secreted sweat is assumed negligible. Moreover, the model minimizes thermal resistance within the body by assuming perfect thermal contact between different tissue groups and assuming that each element emits and absorbs radiation like a black body. Minimizing heat sinks favors accumulation of heat in the body and reducing thermal resistance between tissues facilitates distribution of this heat to the core tissue. These aspects of the model may cause the predicted rise in core temperature due to heat entering the body at the surface of the skin to be greater than that which occurs in the true physical system.

The accuracy of spatial temperature variation is limited in this model. Singularities are produced in the function that approximates the integral of the energy balance when *n* becomes too large. Radiative and conductive heat exchange in and out of each shell is proportional to the surface area of the shell and independent of its volume. At larger values of *n*, the volume of each shell approaches zero. Concurrently, the surface area of each shell remains near constant and, thus, radiative and conductive heat transfer in and out of the shell remains finite. This skews the temperature of each shell toward infinity, causing the series approximation to diverge as *t* becomes larger. This effect occurs at earlier values of *t* in the n^{th} shell of the skin tissue, which experiences large radiative and conductive heat fluxes imposed on it by the surroundings. To avoid this phenomena, the value of *n* must be one when the finite volume method is applied to the skin tissue and ≤ 2 when it is applied to the other tissue groups. This limits the number of discrete points within the body at which temperature can be approximated, reducing the accuracy of modeled spatial temperature variation.

Results and Discussion

I. Control Trial

Blue light spectral irradiance was set to zero during the control trial. The value of *n* was set equal to 1 for the skin and 2 for the remaining tissue groups. The total time was set equal to 24 h, the length of phototherapy during the clinical study done by Aydemir et al [4]. The average temperature of each tissue group was calculated at each time point. Solutions and plots were generated using Matlab R2015. A copy of the code is found below.

Average core temperature dropped during the first 15 min, rose for 45 min, dropped again and leveled off between 5-10 h to a near constant value of 36.9 °C for the remaining time. Average muscle and bone tissue temperatures rose during the first 5 h and then dropped. Both leveled off in the range of 37-37.3 °C. Average skin temperature dropped sharply from 37 to 34.4 °C within the first 3 h and leveled off at 34.4 °C for the remainder of time. Average fat and connective tissue temperatures both dropped sharply during the first 3 h and leveled off to 36.2 °C and 35.3 °C, respectively. Figure 5 exhibits the data.

Skin tissue temperature may have dropped sharply due to rapid heat exchange with the relatively cool environment. Direct heat exchange with the environment occurred only at the skin layer. Average core, fat, and connective tissue temperatures all dropped during the first 30 min. Fat and connective tissue are relatively close to the skin layer and may have experienced a sharp decline in temperature during the first hour due to conductive heat loss to the skin. Core tissue receives blood equilibrated to the temperature of skin, fat, and connective tissue. The initial drop in average core temperature may have occurred due to convective heat loss to the cold blood arriving from these peripheral tissue groups. The trend of average bone and muscle temperature contrasts with that exhibited by the other tissue groups. The muscle shell lies adjacent to and below the connective tissue shell, which exhibited an initial drop in temperature. However, basal metabolic heat production and basal blood perfusion rate are higher in muscle tissue relative to connective tissue. Moreover, the volume of the muscle tissue shell is over six times greater than that of the connective tissue shell. These factors may explain the initial rise in muscle temperature

despite its proximity to the colder connective tissue. The bone shell lies under the warm muscle and above the core, relatively far from major sinks of heat. It is possible that bone tissue temperature rose initially and remained higher than that of other tissue groups due to its position.

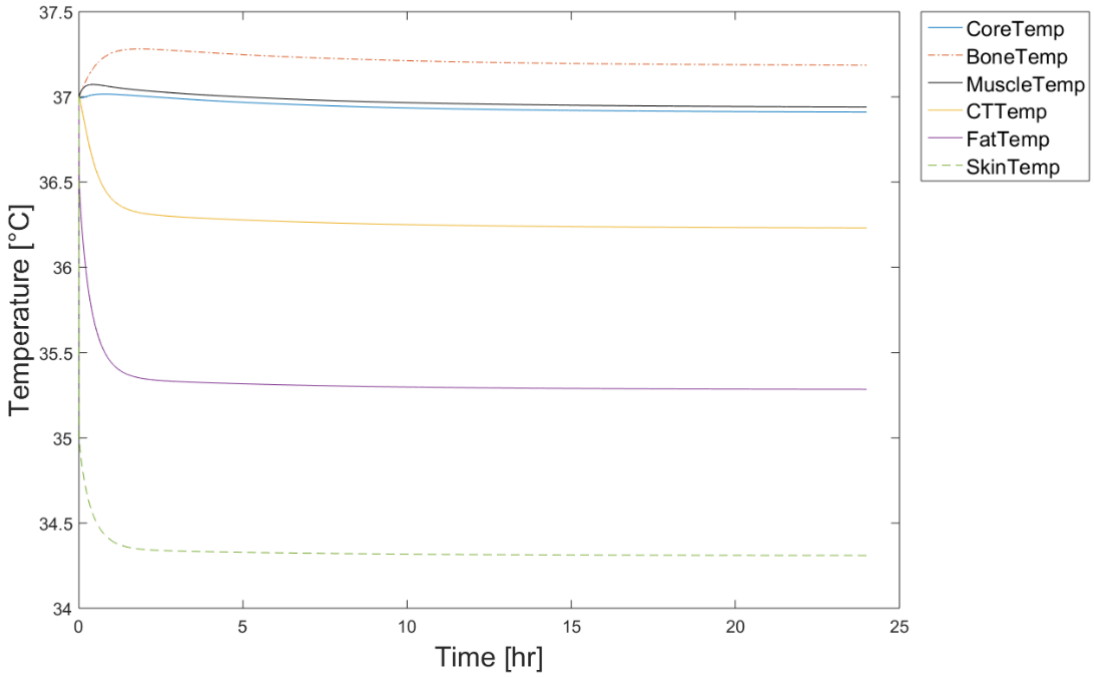

Figure 5. Average temperature of each tissue group calculated by the model over a 24 h period is shown. Blue light spectral irradiance is set to zero. Average core temperature dropped slightly during the first 30 min, rose for a short time, and leveled off at 36.9 °C. Average bone and muscle temperatures rose during the first 3 h and then leveled off to within the range of 37-37.3 °C. Average connective, fat, and skin tissue temperatures fell during the first 3 h and then leveled off at a value of 36.2 °C, 35.3 °C, and 34.4 °C, respectively.

Results from the control trial may suggest that the model reasonably approximates temperature variation within a neonate placed in an incubator environment. Neonatal incubators are designed to maintain the patient in normothermia. The value of normal core body temperature is in the range of 36.5-37.5 °C [19] [23]. The average temperature of core structures approximated by the model remains within this range at all time points. Moreover, values of mean skin temperature of healthy 4-5 day old neonates in an incubator are in the range of 33.9-34.5 °C per data collected by others [7]. Average skin temperature calculated by the model leveled off within this range despite the fact that initial skin temperature was set to 37 °C.

II. Experimental Trial

Average core tissue temperature was modeled using different values of blue light spectral irradiance. Blue light spectral irradiance was set to 0, 10, 30, 60, 120 and 200 μW-cm^{-2}-nm^{-1} in separate trials. Solutions and plots were generated using Matlab R2015. A copy of the code is found below.

Average core temperature dropped during the first 15 min, rose over the next 45 minutes, fell and leveled off to a steady value in each trial aside from the 200 μW-cm^{-2}-nm^{-1} trial. It dropped during the first 15 min and rose until 23 h in the 200 μW-cm^{-2}-nm^{-1}. The value of average core temperature in every trial remained in between 36.9-37.1 °C during the entire 24 h. The trend of average core temperature in each trial is shown in Figure 6. Table 3 gives average core temperature after 24 h in each trial.

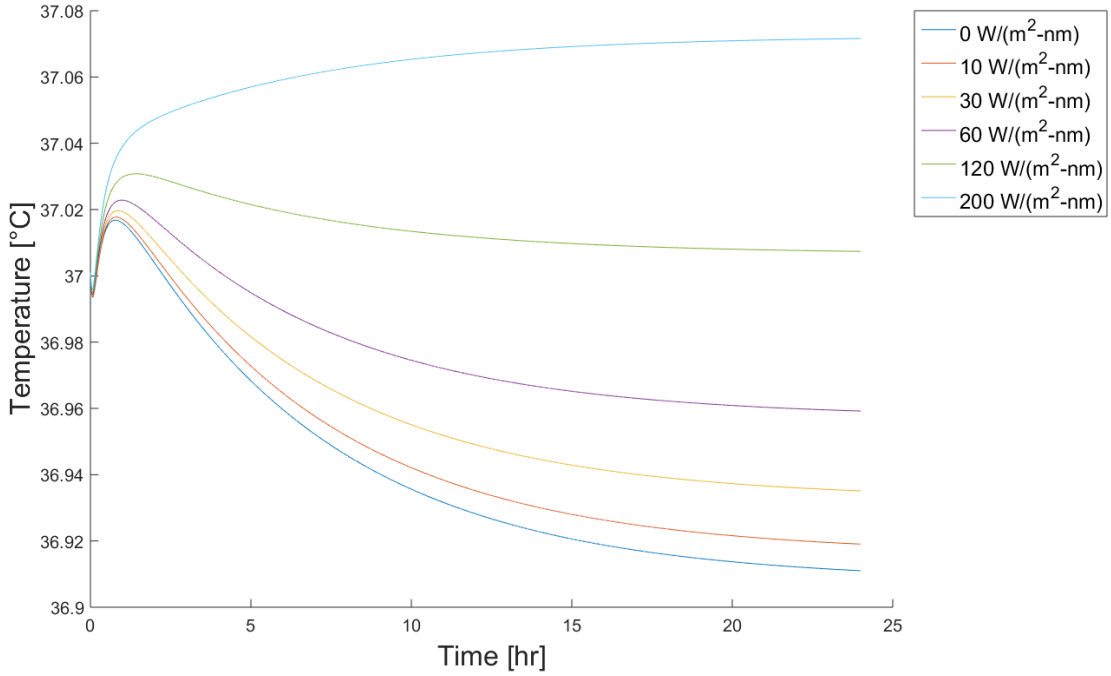

Figure 6. Average core temperature was modeled at different values of blue light spectral irradiance. Average core temperature leveled off between 36.9-37.1 °C when spectral irradiance was set to 0, 10, 30, 60, 120 and 200 μW-cm^{-2}-nm^{-1}. Core temperature dropped during the first 15 min, rose for the next hour, dropped and leveled off in all trials aside from the 200 μW-cm^{-2}-nm^{-1} trial. Core temperature dropped during the first 15 min and rose for the next 23 h in the 200 μW-cm^{-2}-nm^{-1} trial.

Table 3. Values of average core temperature after 24 h modeled for different values of blue light spectral irradiance.

Blue light Spectral Irradiance [μW-cm^{-2}-nm^{-1}]	Average Core Temperature at 24 h [°C]
0	36.91
10	36.92
30	36.94
60	36.96
120	37.01
200	37.07

Trials were conducted at higher values of blue light spectral irradiance. Average core body temperature exceeded 37.5 °C within the 24 h time window only when spectral irradiance was set to a value ≥760 μW-cm^{-2}-nm^{-1}. Data from these trials is not shown.

Modeled core temperature variation contrasted with body temperature trends observed in the clinical setting. Aydemir et al. demonstrated that axillary temperature was ≥37.5 °C in neonates irradiated with blue light at a spectral irradiance ≥60 μW-cm^{-2}-nm^{-1}. The temperature of core body structures is best approximated via rectal thermometry, and axillary temperature underestimates rectal temperature by 0.3 °C on average [19]. Average core tissue temperature approximates core structure temperature in the model, and the value of this is less than 37.5 °C when spectral irradiance is set to a value less than 760 μW-cm^{-2}-nm^{-1}. This contrast may suggest that blue light absorption does not significantly raise the body temperature of a neonate undergoing intensive blue light phototherapy and that other sources of heat not considered by the model may be present in the true physical system.

Conclusion

Predictions offered by the model suggest that absorption of blue light does not increase the body temperature of a neonate during intensive blue light phototherapy to the degree observed in the clinical setting. These predictions are in spite of the fact that assumptions made during the development of the model favor accumulation of heat within the body. Heat generating biologic processes, such as the previously proposed cytokine mediated inflammatory process, may be triggered during intensive blue light phototherapy and may lead to more drastic elevations in body temperature. Future models may consider incorporating the effects of such biologic processes to further investigate this possibility.

Endnotes

1. Ahn, Y., & Garruto, R. (2008). Estimations of body surface area in newborns. *Acta Pediatrica*, 366–370.
2. Anderson, & Parrish. (1981). The Optics of Human Skin. *The Journal of Investigative Dermatology*, 13-19.
3. Apedoh, & et al. (1999). Mannequin-Assessed Dry-Heat Exchanges in the Incubator-Nursed Newborn. *Biomedical Instrumentation Technology*, 446-454.
4. Aydemir, O & et al. (2014). Body temperature changes of newborns under fluorescent versus LED phototherapy. *Indian Journal of Pediatrics*, 751-754.
5. Balaji, C. (n.d.). Mod-01 Lec-39 Transient conduction. Department of Mechanical Engineering, IIT Madras: https://www.youtube.com/watch?v=G8oW5KQHcvQ.
6. Chen, M. (1985). The Tissue Energy Balance Equation. In A. Shitzer, & R. Eberhart, *Heat Transfer in Medicine and Biology* (pp. 153-164). New York: Plenum Publishing Corporation.
7. Clark, R., & Stothers, J. (1979). Neonatal Skin Temperature Distribution Using Infra-Red Colour Thermography. *Journal of Physiology*, 323-333.
8. Ferreira, & Yanagihara. (1999). A thermoregulatorymodel of the human body: exposure to hot environment. *Brazilian Journal of Biomedical Engineering*, 87–96.
9. Ferreira, & Yanagihara. (2009). A transient three-dimensional heat transfer model of the human body. *International Communications in Heat and Mass Transfer*, 718–724.
10. Friis-Hansen, B. (1963). The Body Density of Newborn Infants. *Acta Pediatrica*, 513-521.
11. Gagge, Stolwijk, & Nishi. (1971). An effective temperature scale based on a simple model of human physiological regulatory response. *ASHRAE Transactions*, 247–262.
12. Hansen, T. (2016, March 04). *Neonatal Jaundice*. Retrieved from Medscape: http://emedicine.medscape.com/article/974786-overview#a5
13. Lamola, A. (2016). A Pharmacologic View of Phototherapy. *Clinics in perinatology*, 259-276.
14. Maisels, & McDonagh. (2008). Phototherapy for Neonatal Jaundice. *The New England Journal of Medicine*, 920-928.
15. Management of Hyperbilirubinemia in the Newborn Infant 35 or More. (2004). *Pediatrics (American Academy of Pediatrics)*, 297-316.
16. *Newborn Measurements*. (2017). Retrieved from University of Rochester Medical Center: Health Encyclopedia:

https://www.urmc.rochester.edu/encyclopedia/content.aspx?contenttypeid=90&contentid=P02673

17. Nielsen, K., & et al. (2008). The optics of human skin: Aspects important for human health. *The Norwegian Academy of Science and Letters*, 35-46.
18. Pennes, H. (1948). Analysis of Tissue and Arterid Blood Temperatures in the Resting Human Forearm. *Journal of Applied Physiology*, 93-122.
19. Placidi, G., Merusi, I., & Gagliardi, L. (2014). Rectal, Axillary or Skin Temperature in Newborns? *Journal of Pregnancy and Child Health*.
20. Sanchez-Marin, F., Calixto-Carrera, S., & Villasenor-Mora, C. (2009). Novel approach to assess the emissivity of the human skin. *Journal of Biomedical Optics*.
21. Shitzer, A., & Eberhart, R. (1985). *Heat Transfer in Medicine and Biology.* New York: Plenum Publishing Corporation.
22. Steketee, J. (1973). Spectral Emissivity of Skin and Pericardium. *Physics in Medicine and Biology*, 686-694.
23. *Thermal Protection of the Newborn: a practical guide.* The World Health Organization (1997)
24. Werner, J., & Buse, M. (1988). Temperature profiles with respect to inhomogeneity and geometry of the human body. *American Physiological Society*, 1110-1118.

Assumptions

The following assumptions were made during the model development. Each assumption is listed according to the subsection in which it was incorporated in the model.

Physical System and Surroundings:

- A single cylinder composed of a circular central cylinder circumscribed by five concentric shells reasonably approximates the neonatal body.
- Each tissue group is in perfect thermal contact with the tissue group adjacent to it.
- The values of physical properties, basal metabolic heat production and volume fraction of different body parts measured in the adult body reasonably approximate those values in the neonatal system.
- All tissue groups are initially at a temperature of 37 °C.
- The temperature of the blanket, walls and air in the incubator are at a constant temperature of 33 °C.
- The air inside the incubator is stagnant.
- The incubator walls circumscribe the neonate.
- The blanket covers half the body surface area of the neonate.
- Non-radiative heat generated by the blue light source does not reach the neonate body.

General Model Development

- Bulk kinetic energy and net chemical potential energy are constant.
- Work is not done.
- Temperature is independent of longitudinal position and azimuthal angle.
- Basal metabolic heat production rate is constant within each tissue type.
- The ends of the cylinder are perfectly insulated.
- Density, heat capacity and volume are independent of time.

Convective Heat Transfer

- Blood flowing away from a tissue element is at the temperature of the tissue element it exited.
- Convective heat exchange due to bulk blood flow is negligible.
- Basal blood perfusion rate is constant for a given tissue type.
- Air is stagnant.
- The overall heat transfer coefficient describing natural convective heat loss between the skin and the air is constant.

Radiative Heat Transfer

- All radiation absorbed by the skin ultimately takes on the form of heat.
- Reflection of blue light by the skin is diffuse at all wavelengths.
- Absorptivity of skin in the IR spectrum is one and constant.
- The walls of the incubator and the blanket emit radiation like black bodies.

- The view factor governing radiative heat exchange between the skin and the surrounding matter is equal to one.
- Radiation emitted by all tissue types is completely diffuse.
- Emissivity of all tissue groups is one and constant.

Heat exchange due to evaporation of water

- Heat loss due to evaporation of secreted sweat is negligible.
- The Antoine equation reasonably approximates the vapor pressure of water as a function of temperature.

Variable notation and units

- A: Lateral surface area [m^2]
- B: Basal metabolic heat production [W/m^3]
- B_{micro}: Heat exchange between the tissue and blood in the capillaries per unit volume of tissue [W/m^3]
- BSA: Body surface area [m^2]
- c_{bl}: Specific heat capacity of blood [J/kg-K]
- C_p: Specific heat capacity [J/kg-K]
- E_{sk}: Total evaporative heat loss from the skin [W]
- E_{diff}: Heat loss due to diffusion of water from the skin to the bulk air [W]
- E_{sw}: Heat loss due to evaporation of secreted sweat[W]
- F_{pcl}: Permeation efficiency of water through clothes
- H: Net rate of heat entering the system [W]
- h: Overall heat transfer coefficient [W/m^2-K]
- i: This symbol denotes an arbitrary volume element in the series of elements numbered from 1 to n that make up the discretized body.
- I: Spectral irradiance [W/m^2-nm]
- J: Conductive heat flux [W/m^2]
- k: Thermal conductivity [W/m-K]
- L: Length of the simplified body [m]
- m: Mass of the system [kg]
- M_{surr}: Monochromatic emissive power of the walls and blanket [W/nm-m^2]
- n: Number of elements in the discretized body
- P: Planck's Law [W/sr- m^2-nm]
- p_i: Midpoint of the i^{th} element [m]
- P_{sk}: Vapor pressure of water at skin temperature [mmHg]
- P_a: Vapor pressure of water in bulk air [mmHg]
- Q: Convective heat transfer [W/m^3]
- r: Radius [m]
- r_i: Outer radius of the i^{th} element [m]
- Δr: Width of every element in the discretized body [m]
- R: Radiative heat flux [W/m^2]
- R_b: Rate of heat flux entering the skin via absorption of blue light radiation [W/m^2]
- R_B: Rate of heat entering the skin via absorption of blue light radiation [W]
- R_{surr}: Heat flux entering the neonate as radiation emitted by the walls and blanket [W/m^2]
- $R_{surr,total}$: Heat entering the neonate as radiation emitted by the walls and blanket [W]
- R_t: Radiative flux emitted by the tissue element [W/m^2]
- t: Time [s]
- t_f: Final time (bound of integration) [s]
- t_i: Initial time (bound of integration) [s]
- T: Temperature [K]
- T_a: Temperature of arterial blood [K]
- T_v: Temperature of venous blood [K]
- T_s: Temperature of the skin surface [K]
- $T_{skin,avg}$: Average skin temperature [K]
- T_∞: Temperature of bulk air, wall and blanket [K]
- U: Internal energy [J]
- V: Volume [m^3]
- V_i: Volume of the i^{th} element [m^3]
- W: Rate of work done on the system [W]
- w_{diff}: Skin dampness factor
- z: Longitudinal position [m]

Greek symbols

- α: Absorptivity of skin
- γ: Reflectivity of skin
- ε: Emissivity
- θ: Polar angle
- κ: Proportionality constant relating vapor pressure to evaporative heat loss [°C/mmHg]
- λ: Wavelength [nm]
- λ_f: Upper bound of wavelength (bound of integration) [nm]
- λ_i: Lower bound of wavelength (bound of integration) [nm]
- Π: Pi
- ρ: Density [kg/m^3]
- ρ_{bl}: Density of blood [kg/m^3]
- σ: Stefan-Boltzmann constant [$J/K^4\text{-}m^2$]
- τ: Transmissivity of skin
- φ: Azimuthal angle
- φ_a: Relative humidity of bulk air
- ω_{bl}: Basal blood perfusion rate [$m^3_{blood}/s\text{-}m^3_{tissue}$]

Code

The following is the Matlab R2015 code used to calculate the temperature profile in each tissue. Plot commands are not included. The model is solved by running the mainfn file.

mainfn:

```
clc

% Temperature model of a neonatal human undergoing blue light
% phototherapy for management of hyperbilirubinemia

% A physical representation of the model and assumptions made during the
% development of the model are given above.

% The scalar 't' is the magnitude of the time domain in [s] and 'deltat'
% is the time interval over which change in temperature is approximated.

t=24*60*60;

deltat=1;

% 'Vtotal' is the volume of the neonatal body in [m^3].

Vtotal=0.0031;
Vcore=0.152*Vtotal;
Vbone=Vtotal*0.12;
Vmuscle=Vtotal*0.441;
Vct=0.069*Vtotal;
Vfat=0.162*Vtotal;
Vskin=0.053*Vtotal;

% 'BSA' is the body surface are of the neonate, calculated using the Meban
% formula, in [m^2]

BSA=0.21;

% 'L' is the length of the approximated neonatal body in [m]

L=1.11;

% The radius of the central cylinder and of the outer radius the
% concentric shells representing bone, muscle, connective, fat, and skin
% tissue are 'Rcore', 'Rbonetissue', 'Rmuscle', 'Rct', 'Rfat', and 'Rskin',
% respectively'.

Rcore=(Vcore/(pi*L))^(1/2);
Rbone=((Vcore+Vbone)/(pi*L))^(1/2);
Rmuscle=((Vcore+Vbone+Vmuscle)/(pi*L))^(1/2);
Rct=((Vct+Vcore+Vbone+Vmuscle)/(pi*L))^(1/2);
Rfat=((Vfat+Vct+Vcore+Vbone+Vmuscle)/(pi*L))^(1/2);
```

```
Rskin=((Vskin+Vfat+Vct+Vcore+Vbone+Vmuscle)/(pi*L))^(1/2);

% Each tissue element is divided into 'n' number of finite elements. The variable
% ncore is equal to n and describes the number of discretized elements in the
% core. Note that n is not used in the calculation of skin temperature. Skin is
% treated as a lumped system.

n=2;
ncore=n;

% The temperature of each finite elements in the core, bone, muscle,
% connective, fat and skin tissue are given by the matrices 'Tcore',
% 'Tbone', 'Tmuscle', 'Tct', 'Tfat', and 'Tskin', respectively, in units
% of [K]. The rows of each matrix defines the position of each finite
% element within each tissue group. The columns of the temperature matrix is
% the time axis and the time lapse from one column to the next is equivalent
% to 'deltat'. Zeros are used as place holders in each temperature matrix.
% Calculated values of temperature are inputted by the other m.files.

Tcore=zeros(n,t);
Tbone=zeros(n,t);
Tmuscle=zeros(n,t);
Tct=zeros(n,t);
Tfat=zeros(n,t);
Tskin=zeros(1,t);

% Each finite element in each tissue group is set to an initial temperature
% of 310 [K], consistent with the assumption that initial temperature is
% uniform.

Tcore(:,1)=37+273;
Tbone(:,:)=37+273;
Tmuscle(:,:)=37+273;
Tct(:,:)=37+273;
Tfat(:,:)=37+273;
Tskin(:,:)=37+273;

% Approximated temperature values are inputted into the temperature matrices
% by the following m.files. There is a separate m.file for each tissue group.
% These files are repeated over the domain of time to calculate
% temperature approximations over the entire time domain. The variable 'tt'
% is the array of time points being approximated.

for tt=1:t

corefn;
bonetissuefn;
musclefn;
ctfn;
fatfn;
skinfn;

end

hold off
```

```
x=1:1:t;
y=x/3600;

% The matrices CoreTemp, BoneTemp, MuscleTemp, CTTemp, FatTemp, and SkinTemp
contain the mean value of temperature averaged over all discrete elements in
each tissue group at every time point.

CoreTemp=sum(Tcore(:,x))/n-273;
BoneTemp=sum(Tbone(:,x))/n-273;
MuscleTemp=sum(Tmuscle(:,x))/n-273;
CTTemp=sum(Tct(:,x))/n-273;
FatTemp=sum(Tfat(:,x))/n-273;
SkinTemp=Tskin(:,x)-273;
```

corefn:

```
% Temperature approximation of all finite elements within the core tissue is
calculated by this file.

clear i ii deltar p r k Cp w

% 'i' is a spatial index that defines the position of the finite
% element in the tissue type being evaluated.

i=1:n;

% 'p' is density in [kg/m^3]. 'Cp' is specific heat capacity
% [J/(kg-K)]. 'k' is thermal conductivity in [W/(m-K)]. 'w' is basal blood
% perfusion rate in [m^3 of blood/ (m^3 of tissue-s].

p=970;
Cp=3650;
k=0.47;

% 'o' is the Stefan-Boltzmann constant in [W/(m^2-K^4)]

o=5.67*10^-8;

% Density and specific heat of blood are represented by 'pblood' in [kg/m^3]
% and 'Cpblood' in [J/(kg-K)], respectively.

pblood=1059;
Cpblood=3850;

% 'deltar' is the width of each finite element within the tissue group. 'r'
% is the radius of the outer circle that bounds the finite shell.

deltar=Rcore./n;
r=deltar.*i;

% The mass of blood entering the core tissue is the sum of blood leaving
```

```
% the peripheral tissue groups. 'btotal' is the mass flow rate of blood
% entering the core tissue in units of [kg/s]. The basal perfusion rate of
% core tissue is calculated by dividing 'btotal' by the volume of the core
% tissue. 'wcore' is the basal blood perfusion rate of the core
% The volume of the core tissue element is represented by the variable
% 'Vcore' in units of [m^3].

btotal=(Vmuscle*543*10^-6+Vct*90*10^-6+Vfat*77*10^-6+Vskin*362*10^-6);
Vcore=Rcore^2*pi*L;
wtotal=btotal/Vcore;

% The mass fraction of blood sourced from the bone, muscle, connective,
% fat, and skin tissues are represented by xbone, xmuscle, xct, xfat, and
% xskin. These values are used to calculate the mass weighted average
% temperature of blood entering the core tissue.

xbone=0;
xmuscle=0.87;
xct=0.02;
xfat=0.04;
xskin=0.07;

% The following for loop solves the approximated energy balance around
% each tissue group in each discrete element at the time point defined in the
% mainfn. file. if statements are included to account for differences in heat
transfer for different finite elements. The following coefficients are used:

% A= Conduction term
% B= Convection due to blood flow in the microvasculature
% C= Net heat generated and consumed by basal metabolism
% Rout= Radiation emitted by the finite element
% Rin= Radiation entering the finite element

for ii=1:n

   if ii==1

       A=(1/deltar)*deltat*2*k*r(ii)*(Tcore(ii+1,tt)-Tcore(ii,tt));

B=deltat.*wtotal.*pblood.*Cpblood.*(xbone*sum(Tbone(:,tt))/n+xmuscle*sum(Tmus
cle(:,tt))/n+xct*sum(Tct(:,tt))/n+xfat*sum(Tfat(:,tt))/n+xskin*sum(Tskin(:,tt
))/1-Tcore(ii,tt));
       C=828.*deltat;
       Rout=-(o*Tcore(ii,tt)^4*2*pi*r(ii)*L)/Vcore;
       Rin=(o*Tcore(ii+1,tt)^4*2*pi*r(ii)*L)/Vcore;

       Tcore(ii,tt+1)=Tcore(ii,tt)+(1/p)*(1/Cp)*(A+B+C+Rin+Rout);
   end

  if 1<ii && ii<n

       A=(1/deltar)*deltat*2*k*(r(ii)*(Tcore(ii+1,tt)-Tcore(ii,tt))-r(ii-
1)*(Tcore(ii,tt)-Tcore(ii-1,tt))./(r(ii)^2-r(ii-1)^2);

B=deltat.*wtotal.*pblood.*Cpblood.*(xbone*sum(Tbone(:,tt))/n+xmuscle*sum(Tmus
```

```
cle(:,tt))/n+xct*sum(Tct(:,tt))/n+xfat*sum(Tfat(:,tt))/n+xskin*sum(Tskin(:,tt
))/1-Tcore(ii,tt));
       C=828.*deltat;
       Rout=-(o*Tcore(ii,tt)^4*2*pi*r(ii)*L+o*Tcore(ii,tt)^4*2*pi*r(ii-
1)*L)/Vcore;
       Rin=(o*Tcore(ii+1,tt)^4*2*pi*r(ii)*L+o*Tcore(ii-1,tt)^4*2*pi*r(ii-
1)*L)/Vcore;

       Tcore(ii,tt+1)=Tcore(ii,tt)+(1/p)*(1/Cp)*(A+B+C+Rin+Rout);

  end

  if ii==n

       A=(1/deltar)*deltat*2*k*(r(ii)*(Tbone(1,tt)-Tcore(ii,tt))-r(ii-
1)*(Tcore(ii,tt)-Tcore(ii-1,tt))./(r(ii)^2-r(ii-1)^2);

B=deltat.*wtotal.*pblood.*Cpblood.*(xbone*sum(Tbone(:,tt))/n+xmuscle*sum(Tmus
cle(:,tt))/n+xct*sum(Tct(:,tt))/n+xfat*sum(Tfat(:,tt))/n+xskin*sum(Tskin(:,tt
))/1-Tcore(ii,tt));
       C=828.*deltat;
       Rout=-(o*Tcore(ii,tt)^4*2*pi*r(ii)*L+o*Tcore(ii,tt)^4*2*pi*r(ii-
1)*L)/Vcore;
       Rin=(o*Tbone(1,tt)^4*2*pi*r(ii)*L+o*Tcore(ii-1,tt)^4*2*pi*r(ii-
1)*L)/Vcore;

       Tcore(ii,tt+1)=Tcore(ii,tt)+(1/p)*(1/Cp)*(A+B+C+Rin+Rout);

  end

end
```

bonetissuefn:

```
% Temperature approximation of all finite elements within the bone tissue is
calculated by this file.

clear i ii deltar p r k Cp w

% For definitions and units of i, ii, p, Cp, k, o, pblood, Cpblood, deltar,
% r and w, refer to corefn. file.

i=1:n;

p=1520;
k=0.65;
Cp=1700;
w=0;

pblood=1059;
Cpblood=3850;
```

```
deltar=(Rbone-Rcore)./n;
r=(deltar).*i+Rcore;

o=5.67*10^-8;

Vbone=pi*L*(Rbone^2-Rcore^2);

for ii=1:1:n

    if ii==1

        A=(1/deltar)*deltat*2*k*(r(ii)*(Tbone(ii+1,tt)-Tbone(ii,tt))-
Rcore*(Tbone(ii,tt)-Tcore(n,tt)));
        B=deltat.*w.*pblood.*Cpblood.*(sum(Tcore(:,tt))/n-Tbone(ii,tt));
        C=368.*deltat;
        Rout=-
(o*Tbone(ii,tt)^4*2*pi*r(ii)*L+o*Tbone(ii,tt)^4*2*pi*Rcore*L)/Vbone;

Rin=(o*Tbone(ii+1,tt)^4*2*pi*r(ii)*L+o*Tcore(n,tt)^4*2*pi*Rcore*L)/Vbone;

        Tbone(ii,tt+1)=Tbone(ii,tt)+(1./p).*(1./Cp).*(A+B+C+Rout+Rin);

    end

    if 1<ii && ii<n

        A=(1/deltar)*deltat*2*k*(r(ii)*(Tbone(ii+1,tt)-Tbone(ii,tt))-r(ii-
1)*(Tbone(ii,tt)-Tbone(ii-1,tt))./(r(ii)^2-r(ii-1)^2);
        B=deltat.*w.*pblood.*Cpblood.*(sum(Tcore(:,tt))/ncore-Tbone(ii,tt));
        C=368.*deltat;
        Rout=-(o*Tbone(ii,tt)^4*2*pi*r(ii)*L+o*Tbone(ii,tt)^4*2*pi*r(ii-
1)*L)/Vbone;
        Rin=(o*Tbone(ii+1,tt)^4*2*pi*r(ii)*L+o*Tbone(ii-1,tt)^4*2*pi*r(ii-
1)*L)/Vbone;

        Tbone(ii,tt+1)=Tbone(ii,tt)+(1./p).*(1./Cp).*(A+B+C+Rout+Rin);

    end

    if  ii==n

        A=(1/deltar)*deltat*2*k*(r(ii)*(Tmuscle(1,tt)-Tbone(ii,tt))-r(ii-
1)*(Tbone(ii,tt)-Tbone(ii-1,tt))./(r(ii)^2-r(ii-1)^2);
        B=deltat.*w.*pblood.*Cpblood.*(sum(Tcore(:,tt))/n-Tbone(ii,tt));
        C=368.*deltat;
        Rout=-(o*Tbone(ii,tt)^4*2*pi*r(ii)*L+o*Tbone(ii,tt)^4*2*pi*r(ii-
1)*L)/Vbone;
        Rin=(o*Tmuscle(1,tt)^4*2*pi*r(ii)*L+o*Tbone(ii-1,tt)^4*2*pi*r(ii-
1)*L)/Vbone;

        Tbone(ii,tt+1)=Tbone(ii,tt)+(1./p).*(1./Cp).*(A+B+C+Rout+Rin);

    end
```

```
end
```

musclefn:

```
% Temperature approximation of all finite elements within the bone tissue is
calculated by this file.

clear i ii deltar p r k Cp w

% For definitions and units of i, ii, p, Cp, k, o, pblood, Cpblood, deltar,
% r and w, refer to corefn. file.

i=1:n;

p=1085;
k=0.51;
Cp=3800;
w=p*3/(100*60*1000);

pblood=1059;
Cpblood=3850;

deltar=(Rmuscle-Rbone)./n;
r=(deltar.*i+Rbone);

o=5.67*10^-8;

Vmuscle=pi*L*(Rmuscle^2-Rbone^2);

for ii=1:1:n

    if ii==1

        A=(1/deltar)*deltat*2*k*(r(ii)*(Tmuscle(ii+1,tt)-Tmuscle(ii,tt))-
Rbone*(Tmuscle(ii,tt)-Tbone(n,tt)));
        B=deltat.*w.*pblood.*Cpblood.*(sum(Tcore(:,tt))/n-Tmuscle(ii,tt));
        C=684.*deltat;
        Rout=-
(o*Tmuscle(ii,tt)^4*2*pi*r(ii)*L+o*Tmuscle(ii,tt)^4*2*pi*Rbone*L)/Vmuscle;

Rin=(o*Tmuscle(ii+1,tt)^4*2*pi*r(ii)*L+o*Tbone(n,tt)^4*2*pi*Rbone*L)/Vmuscle;

        Tmuscle(ii,tt+1)=Tmuscle(ii,tt)+(1./p).*(1./Cp).*(A+B+C+Rout+Rin);

    end

    if 1<ii && ii<n

        A=(1/deltar)*deltat*2*k*(r(ii)*(Tmuscle(ii+1,tt)-Tmuscle(ii,tt))-
r(ii-1)*(Tmuscle(ii,tt)-Tmuscle(ii-1,tt)))./(r(ii)^2-r(ii-1)^2);
        B=deltat.*w.*pblood.*Cpblood.*(sum(Tcore(:,tt))/n-Tmuscle(ii,tt));
        C=684.*deltat;
```

```
        Rout=-(o*Tmuscle(ii,tt)^4*2*pi*r(ii)*L+o*Tmuscle(ii,tt)^4*2*pi*r(ii-
1)*L)/Vmuscle;
        Rin=(o*Tmuscle(ii+1,tt)^4*2*pi*r(ii)*L+o*Tmuscle(ii-
1,tt)^4*2*pi*r(ii-1)*L)/Vmuscle;

        Tmuscle(ii,tt+1)=Tmuscle(ii,tt)+(1./p).*(1./Cp).*(A+B+C+Rout+Rin);

    end

    if  ii==n

        A=(1/deltar)*deltat*2*k*(r(ii)*(Tct(1,tt)-Tmuscle(ii,tt))-r(ii-
1)*(Tmuscle(ii,tt)-Tmuscle(ii-1,tt)))./(r(ii)^2-r(ii-1)^2);
        B=deltat.*w.*pblood.*Cpblood.*(sum(Tcore(:,tt))/n-Tmuscle(ii,tt));
        C=684.*deltat;
        Rout=-(o*Tmuscle(ii,tt)^4*2*pi*r(ii)*L+o*Tmuscle(ii,tt)^4*2*pi*r(ii-
1)*L)/Vmuscle;
        Rin=(o*Tct(1,tt)^4*2*pi*r(ii)*L+o*Tmuscle(ii-1,tt)^4*2*pi*r(ii-
1)*L)/Vmuscle;

        Tmuscle(ii,tt+1)=Tmuscle(ii,tt)+(1./p).*(1./Cp).*(A+B+C+Rout+Rin);

    end

end
```

ctfn:

```
% Temperature approximation of all finite elements within the bone tissue is
calculated by this file.

clear i ii deltar p r k Cp w

% For definitions and units of i, ii, p, Cp, k, o, pblood, Cpblood, deltar,
% r and w, refer to corefn. file.

i=1:n;

p=1085;
k=0.47;
Cp=3200;
w=p*0.5/(100*60*1000);

pblood=1059;
Cpblood=3850;

deltar=(Rct-Rmuscle)./n;
r=(deltar.*i+Rmuscle);

o=5.67*10^-8;

Vct=pi*L*(Rct^2-Rmuscle^2);
```

```
for ii=1:1:n

    if ii==1

        A=(1/deltar)*deltat*2*k*(r(ii)*(Tct(ii+1,tt)-Tct(ii,tt))-
Rmuscle*(Tct(ii,tt)-Tmuscle(n,tt)));
        B=deltat.*w.*pblood.*Cpblood.*(sum(Tcore(:,tt))/n-Tct(ii,tt));
        C=369.*deltat;
        Rout=-
(o*Tct(ii,tt)^4*2*pi*r(ii)*L+o*Tct(ii,tt)^4*2*pi*Rmuscle*L)/Vct;

Rin=(o*Tct(ii+1,tt)^4*2*pi*r(ii)*L+o*Tmuscle(n,tt)^4*2*pi*Rmuscle*L)/Vct;

        Tct(ii,tt+1)=Tct(ii,tt)+(1./p).*(1./Cp).*(A+B+C+Rout+Rin);

    end

    if 1<ii && ii<n

        A=(1/deltar)*deltat*2*k*(r(ii)*(Tct(ii+1,tt)-Tct(ii,tt))-r(ii-
1)*(Tct(ii,tt)-Tct(ii-1,tt)))./(r(ii)^2-r(ii-1)^2);
        B=deltat.*w.*pblood.*Cpblood.*(sum(Tcore(:,tt))/n-Tct(ii,tt));
        C=369.*deltat;
        Rout=-(o*Tct(ii,tt)^4*2*pi*r(ii)*L+o*Tct(ii,tt)^4*2*pi*r(ii-
1)*L)/Vct;
        Rin=(o*Tct(ii+1,tt)^4*2*pi*r(ii)*L+o*Tct(ii-1,tt)^4*2*pi*r(ii-
1)*L)/Vct;

        Tct(ii,tt+1)=Tct(ii,tt)+(1./p).*(1./Cp).*(A+B+C+Rout+Rin);

    end

    if  ii==n

        A=(1/deltar)*deltat*2*k*(r(ii)*(Tfat(1,tt)-Tct(ii,tt))-r(ii-
1)*(Tct(ii,tt)-Tct(ii-1,tt)))./(r(ii)^2-r(ii-1)^2);
        B=deltat.*w.*pblood.*Cpblood.*(sum(Tcore(:,tt))/n-Tct(ii,tt));
        C=369.*deltat;
        Rout=-(o*Tct(ii,tt)^4*2*pi*r(ii)*L+o*Tct(ii,tt)^4*2*pi*r(ii-
1)*L)/Vct;
        Rin=(o*Tfat(1,tt)^4*2*pi*r(ii)*L+o*Tct(ii-1,tt)^4*2*pi*r(ii-
1)*L)/Vct;

        Tct(ii,tt+1)=Tct(ii,tt)+(1./p).*(1./Cp).*(A+B+C+Rout+Rin);

    end

end
```

fatfn:

```
% Temperature approximation of all finite elements within the bone tissue is
calculated by this file.

clear i ii deltar p r k Cp w

% For definitions and units of i, ii, p, Cp, k, o, pblood, Cpblood, deltar,
% r and w, refer to corefn. file.

i=1:n;

p=920;
k=0.21;
Cp=2300;
w=p*0.5/(100*60*1000);

pblood=1059;
Cpblood=3850;

deltar=(Rfat-Rct)./n;
r=(deltar.*i+Rct);

o=5.67*10^-8;

Vfat=pi*L*(Rfat^2-Rct^2);

for ii=1:1:n

    if ii==1

        A=(1/deltar)*deltat*2*k*(r(ii)*(Tfat(ii+1,tt)-Tfat(ii,tt))-
Rfat*(Tfat(ii,tt)-Tct(n,tt)));
        B=deltat.*w.*pblood.*Cpblood.*(sum(Tcore(:,tt))/n-Tfat(ii,tt));
        C=300.*deltat;
        Rout=-(o*Tfat(ii,tt)^4*2*pi*r(ii)*L+o*Tfat(ii,tt)^4*2*pi*Rct*L)/Vfat;
        Rin=(o*Tfat(ii+1,tt)^4*2*pi*r(ii)*L+o*Tct(n,tt)^4*2*pi*Rct*L)/Vfat;

        Tfat(ii,tt+1)=Tfat(ii,tt)+(1./p).*(1./Cp).*(A+B+C+Rout+Rin);

    end

    if 1<ii && ii<n

        A=(1/deltar)*deltat*2*k*(r(ii)*(Tfat(ii+1,tt)-Tfat(ii,tt))-r(ii-
1)*(Tfat(ii,tt)-Tfat(ii-1,tt))./(r(ii)^2-r(ii-1)^2);
        B=deltat.*w.*pblood.*Cpblood.*(sum(Tcore(:,tt))/n-Tfat(ii,tt));
        C=300.*deltat;
        Rout=-(o*Tfat(ii,tt)^4*2*pi*r(ii)*L+o*Tfat(ii,tt)^4*2*pi*r(ii-
1)*L)/Vfat;
        Rin=(o*Tfat(ii+1,tt)^4*2*pi*r(ii)*L+o*Tfat(ii-1,tt)^4*2*pi*r(ii-
1)*L)/Vfat;
```

```
        Tfat(ii,tt+1)=Tfat(ii,tt)+(1./p).*(1./Cp).*(A+B+C+Rout+Rin);

    end

    if  ii==n

        A=(1/deltar)*deltat*2*k*(r(ii)*(Tskin(1,tt)-Tfat(ii,tt))-r(ii-
1)*(Tfat(ii,tt)-Tfat(ii-1,tt)))./(r(ii)^2-r(ii-1)^2);
        B=deltat.*w.*pblood.*Cpblood.*(sum(Tcore(:,tt))/n-Tfat(ii,tt));
        C=300.*deltat;
        Rout=-(o*Tfat(ii,tt)^4*2*pi*r(ii)*L+o*Tfat(ii,tt)^4*2*pi*r(ii-
1)*L)/Vfat;
        Rin=(o*Tskin(1,tt)^4*2*pi*r(ii)*L+o*Tfat(ii-1,tt)^4*2*pi*r(ii-
1)*L)/Vfat;

        Tfat(ii,tt+1)=Tfat(ii,tt)+(1./p).*(1./Cp).*(A+B+C+Rout+Rin);

    end

end
```

skinfn:

```
% Temperature approximation of all finite elements within the bone tissue is
calculated by this file.

clear i ii deltar p r k Cp w

% For definitions and units of ii, p, Cp, k, o, pblood, Cpblood, deltar,
% r and w, refer to corefn. file.

% I is the spectral irradiance of blue light [W/m^2-nm]

I=736*10^-6*100^2;

p=1085;
k=0.47;
Cp=3680;
w=p*0.5/(100*60*1000);

pblood=1059;
Cpblood=3850;

deltar=(Rskin-Rfat);
r=Rskin;

o=5.67*10^-8;

Vskin=pi*L*(Rskin^2-Rfat^2);

ii=1;
```

```
% Conduction, convective heat exchange with the blood and
% net metabolic heat generation are described
% as they were for the other tissue groups. Note that 'A' was modified to
% account for conductive heat exchange between the skin and the blanket,
% the latter of which is at a constant temperature of 33 degrees Celsius.
% The variable 'Twall' represents the temperature of the incubator walls
% and the blanket.

Twall=33+273;
A=(1/deltar)*deltat*2*k*(Rskin*(Twall-Tskin(ii,tt))/2-1*Rfat*(Tskin(ii,tt)-
Tfat(n,tt))).(Rskin^2-Rfat^2);
B=deltat.*w.*pblood.*Cpblood.*(sum(Tcore(:,tt))/n-Tskin(ii,tt));
C=368*deltat;

%0.5*Rskin*(33+273-Tskin(ii,tt))

% The following are factors that were not pertinent to heat transfer of
% other tissue groups:

% The coefficient 'D' represents convective heat transfer with the
% surrounding air. 'Tair' is the temperature of air in [K] and 'h' is the
% convective heat transfer coefficient in [W/m^2-K].

Tair= 33+273;
h= 4.94;
D=-h*BSA*(Tskin(ii,tt)-Tair).*deltat/2;

% 'E' is the blue light incident on and absorbed by the skin.

E=BSA*I*50.28*deltat/2;

% 'F' is the radiative heat emmitted by the surrounding wall and the
% environment added to radiation emitted by the fat layer under the skin.
% 'Twall' is the temperature of the blanket and surrounding walls,
% equal to 33 degrees Celsius.

F=BSA*o*Twall.^4*deltat+(o*Tfat(n,tt)^4*BSA*deltat);

% 'G' is the heat transferred out of the skin as radiation

G=-(2*pi*Rskin*L*o*Tskin(ii,tt).^4+2*pi*Rfat*L*o*Tskin(ii,tt).^4)*deltat;

% Heat loss secondary to diffusive evaporation of water out the skin is
% described by the coefficient 'H'.

H=-BSA*0.06*2.2*(10.^(8.07-1730.63/(233.43+Tskin(ii,tt)-273))-
37.7)*4.94*deltat/2;

Tskin(ii,tt+1)=Tskin(ii,tt)+(1./p).*(1./Cp).*(A+B+C+(1/Vskin)*(D+E+F+G+H));
```